Level Set Segmentation of Retinal OCT Images

Bashir Isa Dodo[1], Yongmin Li[1], XiaoHui Liu[1] and Muhammad Isa Dodo[2]

[1]*Department of Computer Science, Brunel University, U.K.*
[2]*Katsina State Institute of Technology and Management, Katsina, Nigeria*

Keywords: Image Segmentation, Level Set, Evolution Constrained Optimisation, Optical Coherence Tomography.

Abstract: Optical coherence tomography (OCT) yields high-resolution images of the retina. Reliable identification of the retinal layers is necessary for the extraction of clinically useful information used for tracking the progress of medication and diagnosis of various ocular diseases. Many automatic methods have been proposed to aid with the analysis of retinal layers, mainly, due to the complexity of retinal structures, the cumbersomeness of manual segmentation and variation from one specialist to the other. However, a common drawback suffered by existing methods is the challenge of dealing with image artefacts and inhomogeneity in pathological structures. In this paper, we embed prior knowledge of the retinal architecture derived from the gradient information, into the level set method to segment seven (7) layers of the retina. Mainly, we start by establishing the region of interest (ROI).The gradient edges obtained from the ROI are used to initialise curves for the layers, and the layer topology is used in constraining the evolution process towards the actual layer boundaries based on image forces. Experimental results show our method obtains curves that are close to the manual layers labelled by experts.

1 INTRODUCTION

Optical coherence tomography first introduced by (Huang et al., 1991) is a noninvasive imaging technique that provides cross-sectional images of the retina with an acquisition speed of approximately 25,000 A-scans per second, and an axial image resolution of approximately 5-7μm (Raftopoulos and Trip, 2012; Jaffe, 2012; Adhi and Duker, 2013). In current ophthalmology, identifying various layers of the retina on OCT has become a vital tool for diagnosing and tracking the progress of medication of various visual impairments (Adhi and Duker, 2013). Since the manual segmentation is not only tedious but also subjected to intra- and inter-grader variance (Yazdanpanah et al., 2011), many automatic methods have been proposed to assist with the segmentation process(Sun et al., 2016). Current research in retinal OCT segmentation focuses on improving various aspects ranging from computational time, the number of layers segmented, use of prior knowledge and computational complexity to mention a few. In general, segmentation is partitioning based on some image characteristics. How these characteristics are defined determines the computation burden of the algorithm. In some cases, this computational burden is reduced through dynamic programming (Chiu et al., 2010) or topology modification (Liu et al., 2018). The number of questions (conditions) an algorithm has to check or satisfy is usually the most crucial factor.

Particularly, Markov Boundary Model (Koozekanani et al., 2001), later extended by (Boyer et al., 2006), geodesic distance (Duan et al., 2017), level sets (Wang et al., 2015; Novosel et al., 2013), graph-based methods (Chiu et al., 2010; Garvin, 2008; Dodo et al., 2017; Dodo et al., 2018), and machine learning (Lang et al., 2013) have been used in the segmentation of retinal OCT images. Although the level sets method has automatic topological handling, the steps can be computationally expensive (Shi and Karl, 2005), while adding complex constraints in the segmentation method usually increases the complexity of an algorithm. In this work, we incorporate simple yet efficient topological constraints to the evolution process of the level set method, to improve accuracy and reduce computational complexity for OCT image segmentation.

The method we propose is based on the following considerations: 1. The image gradients are used to initialise curves in order to handle under-segmentation and over-segmentation of the image; 2.

49

The evolution of a curve is explicitly based on layer arrangements and implicitly based on OCT topology. This means for each image the initial contours are specific to the image under investigation, while the forces in the normal direction and the topology constrains guide the contours towards layer boundaries.

Our method segments an OCT image into 7 segments, relating to: Nerve Fibre Layer (NFL); Ganglion Cell Layer + Inner Plexiform Layer + Inner Nuclear Layer (GCL+IPL+INL); Outer Plexiform Layer (OPL); Outer Nuclear Layer to Inner Segment (ONL+IS), Outer Segment (OS) and Retinal Pigment Epithelium (RPE). Locations of these layers on an OCT image are shown in Figure 1. The rest of the paper is organised as follows. Section 2 discusses the proposed method in details. Experimental results and discussions are treated in Section 3. Finally, conclusions are drawn in Section 4.

2 PROPOSED METHOD

This section describes our approach of segmenting retinal OCT images. A schematic representation of the method is illustrated in Figure 2, and details of each step are elaborated in the subsequent subsections.

2.1 Pre-processing

The pre-processing steps are illustrated in Figure 3. Each OCT B-scan image I is first enhanced with a Gaussian filter to reduce the image noise. The layers targeted in our study lies within the total retinal thickness (TRT), which starts from the Internal Limiting Membrane(ILM) to the posterior boundary of the Retinal pigment epithelium (RPE), i.e. the boundary between the retinal nerve fibre layer and the vitreous, and the boundary between the RPE and the choroid regions respectively. It is commonly accepted that the NFL, IS-OS and RPE exhibits high reflectivity in an OCT image (Chiu et al., 2010; Lu et al., 2011; Tian et al., 2015), based on experiments the ILM and RPE exibits the highest transitions from dark-bright and bright-dark, respectively (Dodo et al., 2018). Based on this understanding of the retinal structure, the ILM and RPE are identified using the shortest path (Dijkstra, 1959), by searching for the highest transitions on two separate adjacency matrices(Chiu et al., 2010).

Using the ILM and RPE points the image is cropped to $I_{cropped}$, such that only the Region of interest (ROI) with useful layer information is remaining. This helps in dealing with layer-like structures

outside the ROI and the computational cost associated with handling image background in segmentation. The pre-processing is vital in our segmentation process because only the actual layer properties impact the evolution of the curve. The next operation on the image is to generate a mask I_{mask} of the cropped image, and then multiply it by the original image I. The examples of resulting images from this step are shown in figure 3, column 4, and expressed by the equation below:

$$I_{processed} = I_{mask} * I \qquad (1)$$

The process in this subsection is essential because only the layer structures are obtained when the gradient of the image is acquired. One of the significant roles of the pre-processing is to eliminate the need for handling background as depicted in figure 4 and further discussed in the next few subsections 2.2 and 2.3. From Figure 4 (a) the background and image noise will affect the segmentation processes (because the area highlighted in red will be initialised), and for this reason we establish the ROI only based on part of the image that contains useful information Figure 4 (b). The estabilishment of the ROI also complements the thresholding and refinement processes in the layer initialisation stage. We use the size of the cropped image to reduce computational time further and to eliminate the need for storing idle points.

2.2 Boundary Initialisation

To initialise contours we obtain the vertical gradient $\nabla I_{processed}$ of the processed image and threshold it by a constant T, in our case $T = 0.0018$. The value of T should ideally be low, to avoid getting more components in the GCL - IPL regions which will negatively impact the segmentation results. We obtain the edges of the thresholded gradient TG image 5(a), and then refine it in two simple steps: first, by area opening ((Vincent, 1994), where any component less than P pixels ($P = 30$pixels) is deleted to remove small objects from the image (most especially the GCL to IPL regions); second, we extrapolate incomplete layer lines to span the image horizontally. This is carried out by linking broken lines to the closet neighbouring points, where each line starts from the first column and ends at the last column of the image, such that only complete layers are initialised, figure 5(b). The initialisation and evolution of complete layer lines exclusively is an essential factor, which further ensures accurate segmentation, i.e. no merging or splitting of boundaries is allowed, which prevents under- or over-segmentation. Without losing context, the refinement step can be ignored, if the layers from the GCL to INL
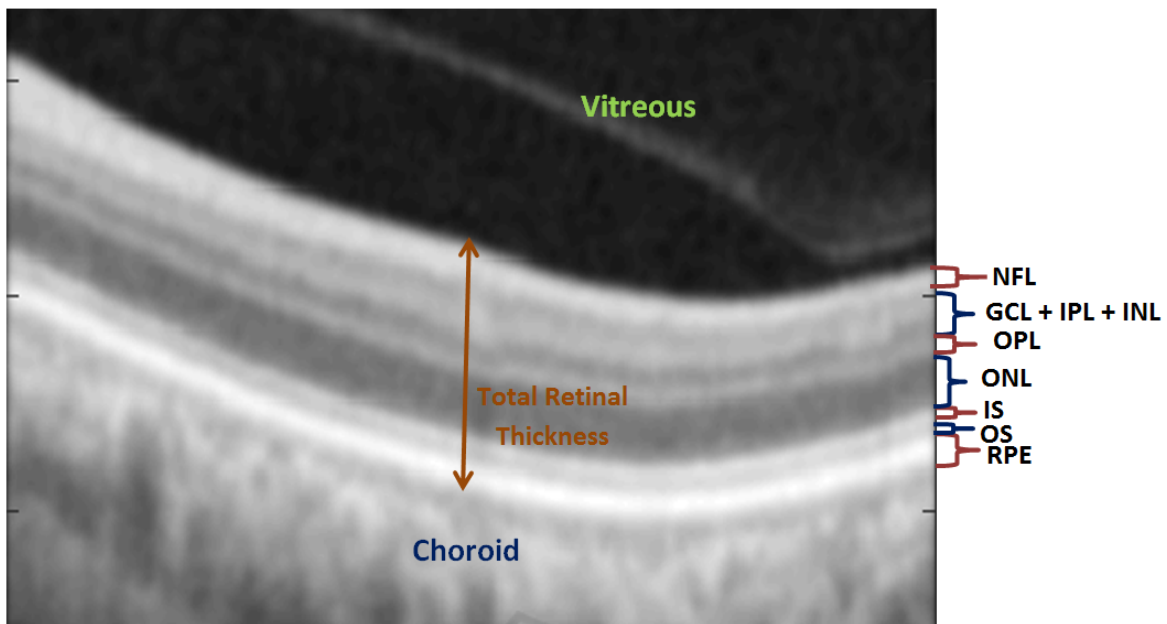
Figure 1: Location of Nerve Fibre Layer (NFL); Ganglion Cell Layer + Inner Plexiform Layer + Inner Nuclear Layer (GCL+IPL+INL); Outer Plexiform Layer (OPL); Outer Nuclear Layer to Inner Segment (ONL+IS), Outer Segment (OS), Retinal Pigment Epithelium (RPE) and the total retinal thickness, on an OCT image.
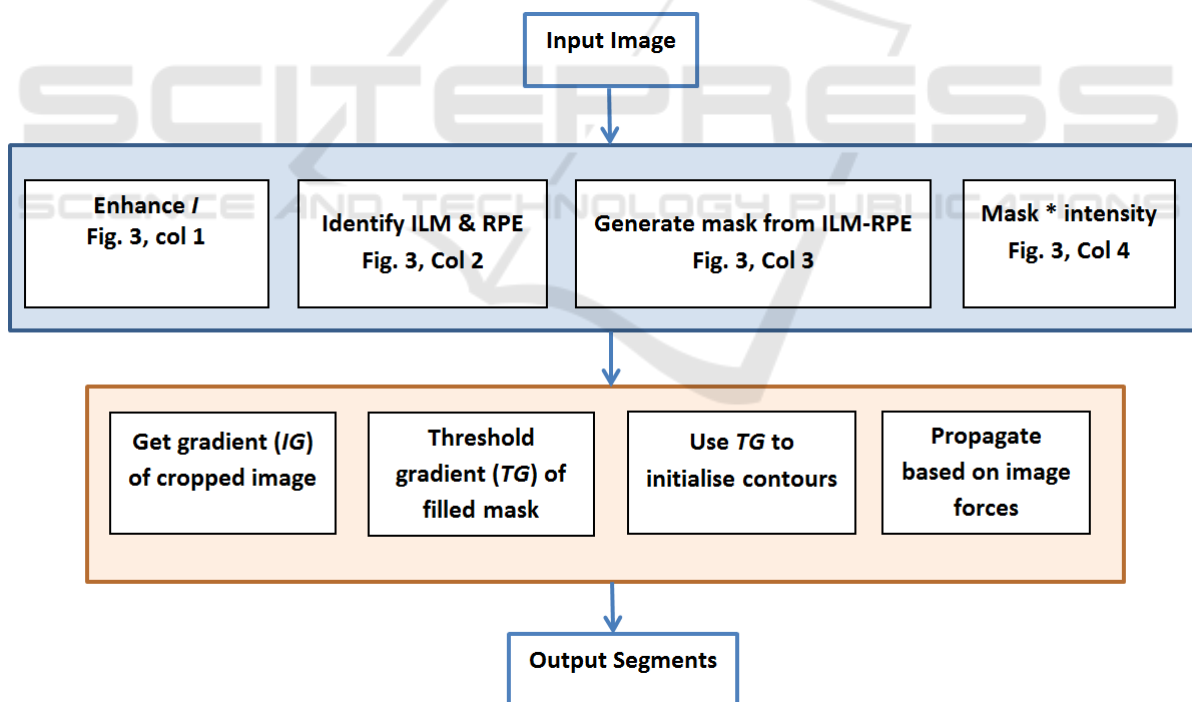
Figure 2: Schematic representation of the proposed level set approach.

are targets of the method. However, this will require a condition for handling the splitting and merging of boundaries or an alternate measure to correctly identify which layers are segmented. Moving further, the edges of the refined image serve as initial curves such

that the number of identified regions in the final output cannot exceed the number of the initial curves. An important point to note is that, if T is reduced, then P is to be increased, mainly because the size of the small objects in 5 (b) will increase with a smaller
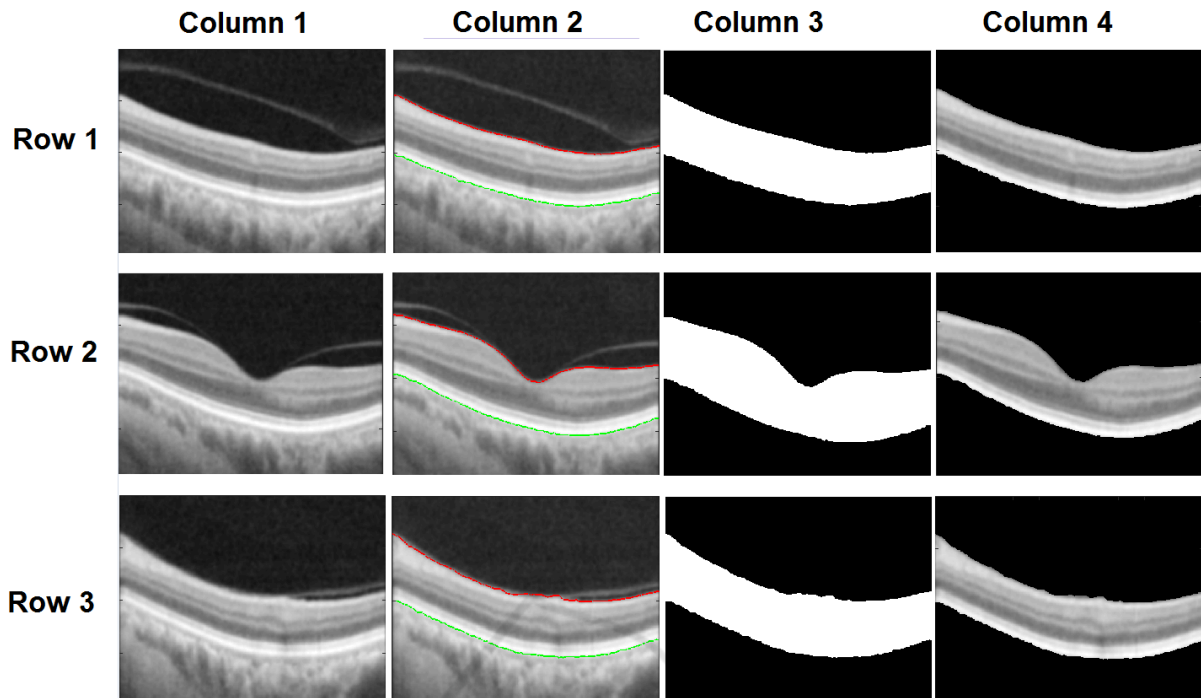
Figure 3: Preprocessing steps showing: Column 1 - Enhanced images; Column 2 - identified ILM (red) and RPE (Green); Column 3 - image masks I_{mask}; and Column 4 - Cropped images $I_{cropped}$. Row 1 - Nasal region; Row 2 - Foveal Region; and Row 3- Temporal Region.
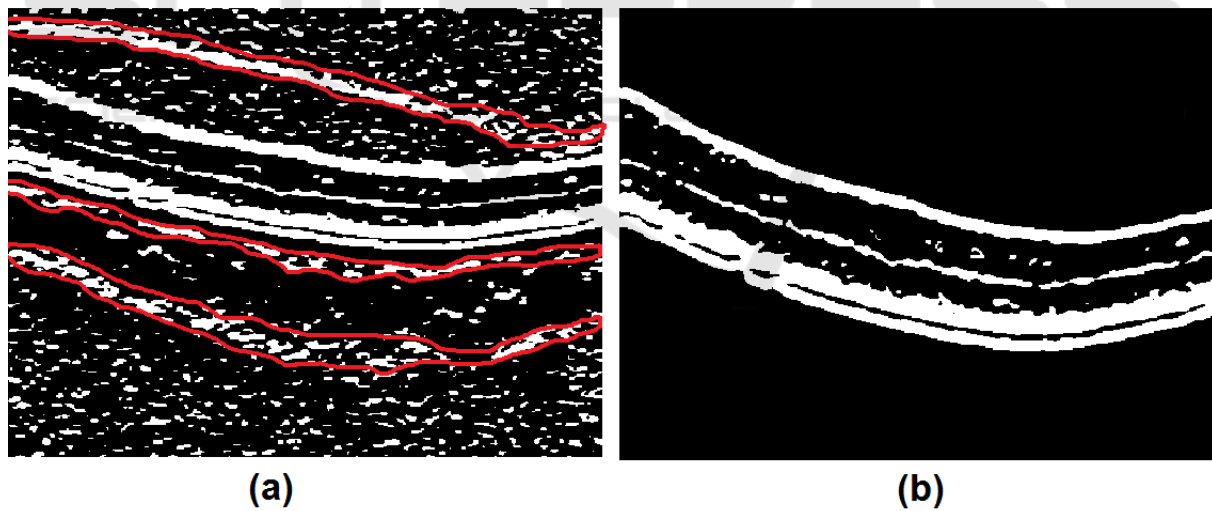
Figure 4: Gradient of full image (Figure - 3 Column 1, Row 1) with background noise and layer-like structures in red (a), and thresholded gradient of preprocessed (Figure 3 - Column 4, Row 1) image TG with ROI only (b).

T. Each boundary curve C_b is therefore represented by a collection of $C_b(x, y)$ on the image.

2.3   Segmentation of OCT

Next, each initial boundary curve C_b is evolved depending on a speed field F based on the following differential equation (Shi and Karl, 2005) :

$$\frac{dC_b}{dt} = F\vec{N} \qquad (2)$$

Where $\vec{N}$ is the normal of the curve pointing outward. The speed field F is made of an external speed derived from the image data and a characteristic speed
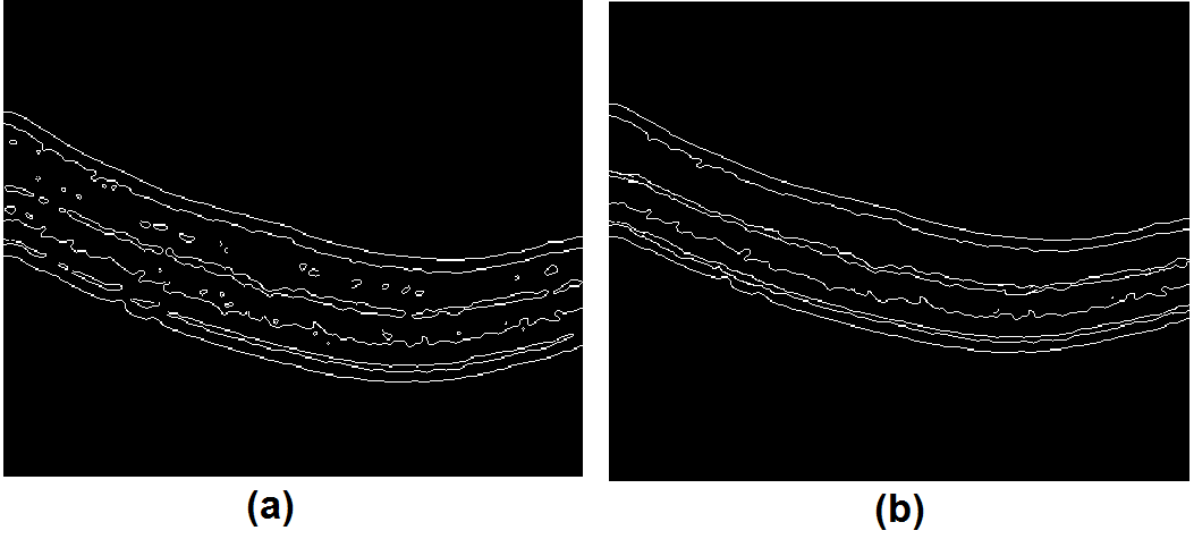
Figure 5: Edges before refinement (a), and refined edges used for contour initialisation (b).

based on C_b. We associate F and the ensuing evolution with a gradient descent solution to solve the minimisation problem based on a Mumford-shah model evolution perspective (Tsai et al., 2001). This means the curve C_b will evolve until it gets to a local minima C_{bmin} of the energy, i.e. static point of the dynamic equation (2). Adapting from (Shi and Karl, 2005), we represent a layer boundary uniquely through two lists of inside L_{in} and outside L_{out} points of C_b. Which are defined as:

$$L_{out} = \{x | \phi(x) > 0 \text{ and } \exists y \in N(x) : \phi(y) < 0\}$$
$$L_{in} = \{x | \phi(x) < 0 \text{ and } \exists y \in N(x): \phi(y) > 0\}$$

where $N(x)$ is a distinct neighbourhood of x, in the level set function ϕ at pixel x. Based on this definition, a positive force switches a point from L_{in} to L_{out} and a negative force switches a point from L_{out} to L_{in}. Each point (x,y) in level set function is defined in relation to the curve C_b as follows (Shi and Karl, 2005):

$$\phi = \begin{cases} 3, & \text{if } x,y \text{ is outside } C_b \text{ and } x,y \notin L_{out}; \\ 1, & \text{if } x,y \in L_{out}; \\ -3, & \text{if } x,y \text{ is inside } C_b \text{ and } x,y \notin L_{in}; \\ -1, & \text{if } x,y \in L_{in}. \end{cases} \quad (3)$$

Based on the definition of ϕ in equation (3), it is undemanding to recognise the location of a point (x,y) on the image in relation to C_b. In our formulation, we use a 2D list to represent initial boundary points, and to save the positions of final boundary points for straightforward mapping in generating the final image output. Alternatively, a 1-D list can be used to save the boundaries point at position ϕ, as

suggested in (Liu et al., 2018). A boundary position (x,y) of ϕ, can either expand or shrink based on:

$$\begin{cases} \text{Expand}(x,y): & C_b(x,y) := C_b(x,y) + 1 \\ \\ \text{Shrink}(x,y): & C_b(x,y) := C_b(x,y) - 1 \end{cases} \quad (4)$$

The evolution of each point is influenced by the image forces computed by a fast gradient vector field(Wang and Boyer, 2012) and the topology constraints to be described in the next subsection 2.4.

2.4 Topology Constrains

As highlighted earlier in subsection 2.1 the ordering of the layers must be preserved. Taking into account the architecture of the OCT image, boundary C_{b2} is always below C_{b1} for any given boundary points C_{b1} and C_{b2}, i.e. a point (x,y) on the curve will neither Shrink nor Expand if it makes $C_{b1}(x,y) \leq C_{b2}(x,y)$. Hence, with our appropriate initialisation, we enforce the topology requirement by carrying out this simple topology validation before either shrinking or expanding a boundary. Finally, we employ an intuitive approach to ensure this topology is preserved, by additionally refining the topology constraint in the vertical direction:

1. Because each layer boundary spans the image horizontally (one boundary point per column) we add a condition for evolving a boundary point $C_b(x,y)$ to a new boundary point $C_{bmin}(x,y)$. We restrict $Expand(x,y)$ if its neighbour points are u consecutive points above it; do not $Shrink(x,y)$ if its neighbour points are u consecutive points below it;

2. Looking at the sample of initial layer boundaries in figure 5, a boundary point $C_b(x,y)$ is limited to a maximum of v operations (either *Expand* or *Shrink*) consecutively in the vertical direction).

The parameters u and v are two prior constants, in our experiments u and v are set to 3 and 20 respectively. The parameter u aids with boundary smoothness and avoiding peaks for $Expand(x,y)$ or valleys for $Shrink(x,y)$ on the boundaries, while v further ensures the layered architecture is preserved. Additionally, this is why our layer initialisation is ideal because the starting points are based on the individual image. The topology constraints facilitate the evolution because the validation is performed before expanding or shrinking a boundary. Perhaps, this might not be ideal for abnormal structures. However, considering the ordering of the layers where C_b2 will always be below C_b1 the layers will move together even in the case of abnormal retinal structure. The pseudo-code of our algorithm is illustrated in Algorithm 1.

3 RESULTS AND DISCUSSIONS

We applied our method to 200 macula OCT images. The original size of each image is 512 by 992 pixels, with a resolution of 16 bits per pixel. We crop the image in the pre-processing stage to improve the results of our method. Comparison to the ground truth labelling is carried out on full image size. In our experiments $N(x) = 8$ neighbourhood, mainly, because only the layers are remaining in the cropped image and the effect of inhomogeneity is reduced. Experimental results show that our method successfully segments seven (7) layers of the retina. Samples of the method output are shown in figure 6.

Table 1 shows the mean and standard deviation for the performance of the method compared to the labelling of manual graders. The values show the promising performance of our method in converging at curves C_{bmin} very close to the actual layer boundaries. Notably, the RNL thickness is used for diagnosing major eye diseases such as glaucoma, and the mean (0.951) and standard deviation (± 0.022) of dice coefficient for this layer is reassuring.

Moreover, it can be deduced that our method is consistent in identifying the layer boundaries from the distribution of the values in figure 7. Considering the second quarterlies of the NFL, IS and RPE begin at ≥ 0.900 further attests to the optimum performance of our method, except for few instances in the GCL+IPL+INL and OPL layers, where the dice score is below 0.800. However, in few instances the method could not properly identify the GCL-INL and
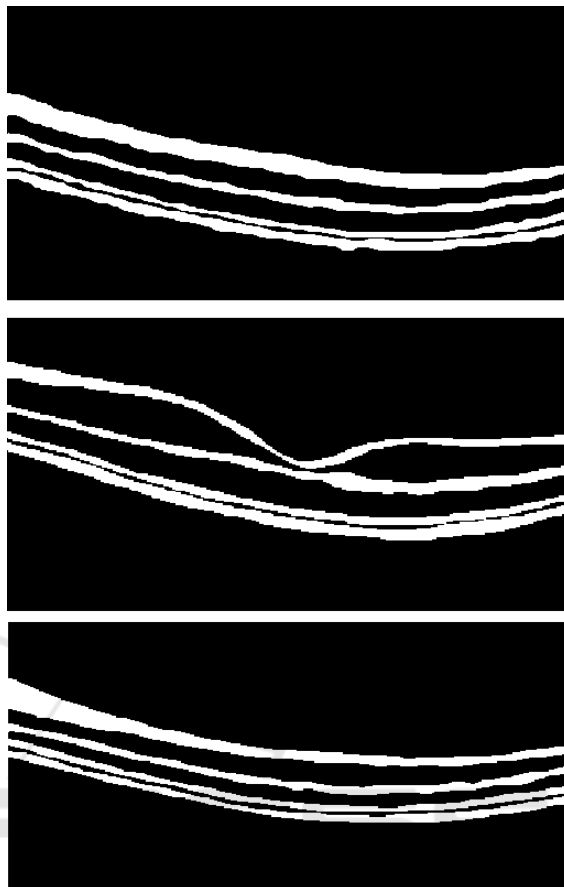
Figure 6: From top to Bottom: Sample results from Nasal, Foveal and Temporal regions respectively.

Table 1: Performance evaluation: Mean and Standard Deviation (STDEV) of Dice Coefficient on 200 B-Scan images (Units in pixels).

RetinalLayer	Mean	STDEV
NFL	0.951	± 0.022
GCL+IPL+INL	0.879	± 0.031
OPL	0.892	± 0.032
ONL	0.907	± 0.030
IS	0.932	± 0.017
OS	0.920	± 0.028
RPE	0.934	± 0.021

the OPL due to some of the small components not been removed. The method avoids over and under segmentation, due to our layer initialisation and topological constraint, which prevents merging or splitting of boundaries. On the other hand, the method will come in short when compared to studies targeting the choroidal region, which is believed to provide details on some of the visual impairments (Sun et al., 2016).

Algorithm 1: Boundary Evolution.

1: Initialise Boundaries
2: *loop:*
3: **if** evolution will not make $C_{b1}(x,y) \leq C_{b2}(x,y)$ **then**
4:     %% Shrink Boundary
5:     **if** neighbours of $C_b(x,y) \neq$ consecutive u points below it **then**
6:       **if** $C_b(x,y)$ has not moved v consecutive points in the vertical direction **then**
7:         **if** force at point is negative **then**
8:           *Shrink*(x,y)
9:     %% Expand Boundaries.
10:     **if** neighbours of $C_b(x,y) \neq$ consecutive u points above it **then**
11:       **if** $C_b(x,y)$ has not moved v consecutive points in the vertical direction **then**
12:         **if** force at point is positive **then**
13:           *Expand*(x,y)
14: %% $C_b(x,y)$ are at relative local minima.
15: **if** no changes made to all $C_b(x,y)$ **then**
16:     *break*
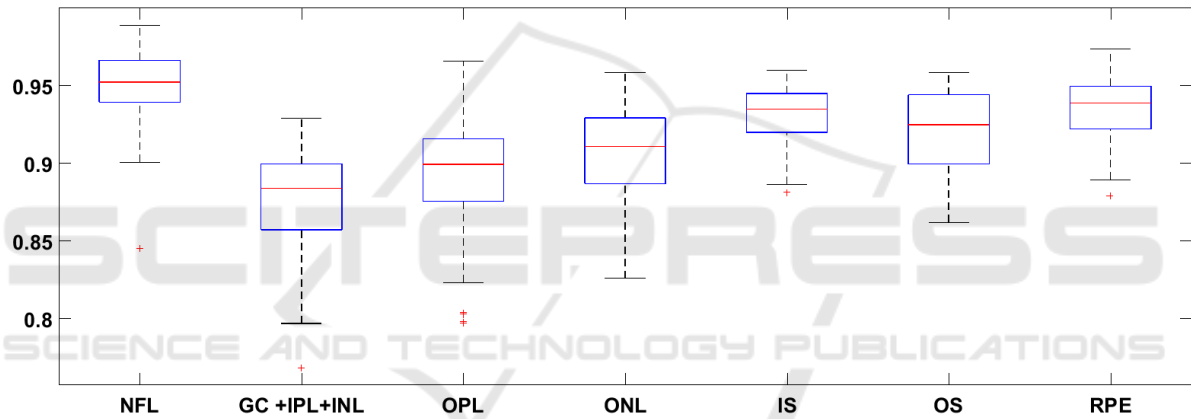
Figure 7: Box plot of mean Dice Coefficient distribution for the seven (7) layers.

4 CONCLUSIONS

We have presented an automatic level set method for retinal OCT segmentation. The proposed work separates retinal OCT images into seven (7) non-overlapping layers. Our approach has explored image segmentation using level set from the point of initialisation, and the constraining of curve evolution based on retinal layer topology explicitly. Refined edges of gradients images are used to initialise the curves. Image forces constrained by the topological architecture of the OCT are used to guide the evolution of the curve to its minimum layer boundaries. These two components ensure the boundaries obtained by the method are close to the actual features of interest. The proposed method takes advantage of handling the obstruction of image background noise in the pre-processing stage, consequently making the segmentation process to suffer less from the image artefacts. Additionally, refinement of the gradient edge information ensures only the targeted layers are initialised at the beginning of the evolution process. Experimental results show that the proposed approach successfully segmented the target layers from OCT images, and the segmentation results are close to the manually labelled ground-truth.Future work will seek to include the GCL to IPL and choroid regions in the ROI, which has to do with implicitly assigning the parameters T and P based on the image as opposed to constants used in our approach.

REFERENCES

Adhi, M. and Duker, J. S. (2013). Optical coherence tomography–current and future applications. *Current*

opinion in ophthalmology, 24(3):213.

Boyer, K. L., Herzog, A., and Roberts, C. (2006). Automatic recovery of the optic nervehead geometry in optical coherence tomography. *IEEE Transactions on Medical Imaging*, 25(5):553–570.

Chiu, S. J., Li, X. T., Nicholas, P., Toth, C. a., Izatt, J. a., and Farsiu, S. (2010). Automatic segmentation of seven retinal layers in SDOCT images congruent with expert manual segmentation. *Optics express*, 18(18):19413–19428.

Dijkstra, E. W. (1959). A note on two problems in connexion with graphs. *Numerische mathematik*, 1(1):269–271.

Dodo, B. I., Li, Y., Eltayef, K., and Liu, X. (2018). Graph-cut segmentation of retinal layers from oct images. In *Proceedings of the 11th International Joint Conference on Biomedical Engineering Systems and Technologies - Volume 2: BIOIMAGING,*, pages 35–42. INSTICC, SciTePress.

Dodo, B. I., Li, Y., and Liu, X. (2017). Retinal oct image segmentation using fuzzy histogram hyperbolization and continuous max-flow. In *2017 IEEE 30th International Symposium on Computer-Based Medical Systems (CBMS)*, pages 745–750. IEEE.

Duan, J., Tench, C., Gottlob, I., Proudlock, F., and Bai, L. (2017). Automated segmentation of retinal layers from optical coherence tomography images using geodesic distance. *Pattern Recognition*, 72:158 – 175.

Garvin, M. K. (2008). Automated 3-D segmentation and analysis of retinal optical coherence tomography images. *PhD thesis - The University of Iowa*.

Huang, D., Swanson, E. A., Lin, C. P., Schuman, J. S., Stinson, W. G., Chang, W., Hee, M. R., Flotte, T., Gregory, K., and Puliafito, C. A. (1991). Optical coherence tomography. *Science (New York, N.Y.)*, 254(5035):1178–81.

Jaffe, G. J. (2012). OCT of the Macula: An expert provides a primer on useful scans, identifying artifacts and time domain vs. spectral domain technology. *Reinal Physician*, pages 10–12.

Koozekanani, D., Boyer, K., and Roberts, C. (2001). Retinal thickness measurements from optical coherence tomography using a Markov boundary model. *IEEE Transactions on Medical Imaging*, 20(9):900–916.

Lang, A., Carass, A., Hauser, M., Sotirchos, E. S., Calabresi, P. a., Ying, H. S., and Prince, J. L. (2013). Retinal layer segmentation of macular OCT images using boundary classification. *Biomedical optics express*, 4(7):1133–52.

Liu, Y., Carass, A., Solomon, S. D., Saidha, S., Calabresi, P. A., and Prince, J. L. (2018). Multi-layer fast level set segmentation for macular oct. In *2018 IEEE 15th International Symposium on Biomedical Imaging (ISBI 2018)*, pages 1445–1448.

Lu, S., Yim-liu, C., Lim, J. H., Leung, C. K.-s., and Wong, T. Y. (2011). Automated layer segmentation of optical coherence tomography images. *Proceedings - 2011 4th International Conference on Biomedical Engineering and Informatics, BMEI 2011*, 1(10):142–146.

Novosel, J., Vermeer, K. A., Thepass, G., Lemij, H. G., and Vliet, L. J. V. (2013). Loosely Coupled Level Sets For Retinal Layer Segmentation In Optical Coherence Tomography. *IEEE 10th International Symposium on Biomedical Imaging*, pages 998–1001.

Raftopoulos, R. and Trip, A. (2012). The Application of Optical Coherence Tomography (OCT) in Neurological Disease. *Advances In Clinincal Neuroscience and Rehabilitation*, 12(2):30–33.

Shi, Y. and Karl, W. C. (2005). A fast level set method without solving pdes [image segmentation applications]. In *Proceedings. (ICASSP '05). IEEE International Conference on Acoustics, Speech, and Signal Processing, 2005.*, volume 2, pages ii/97–ii100 Vol. 2.

Sun, Y., Zhang, T., Zhao, Y., and He, Y. (2016). 3d automatic segmentation method for retinal optical coherence tomography volume data using boundary surface enhancement. *Journal of Innovative Optical Health Sciences*, 9(02):1650008.

Tian, J., Varga, B., Somfai, G. M., Lee, W. H., Smiddy, W. E., and DeBuc, D. C. (2015). Real-time automatic segmentation of optical coherence tomography volume data of the macular region. *PLoS ONE*, 10(8):1–20.

Tsai, A., Yezzi, A., and Willsky, A. S. (2001). Curve evolution implementation of the mumford-shah functional for image segmentation, denoising, interpolation, and magnification. *IEEE Transactions on Image Processing*, 10(8):1169–1186.

Vincent, L. (1994). Morphological area openings and closings for grey-scale images. In *Shape in Picture*, pages 197–208. Springer.

Wang, C., Wang, Y., Kaba, D., Wang, Z., Liu, X., and Li., Y. (2015). Automated layer segmentation of 3d macular images using hybrid methods. In *Proc. International Conference on Image and Graphics. Tianjing, China.*, volume 9217, pages 614–628.

Wang, Q. and Boyer, K. L. (2012). The active geometric shape model: A new robust deformable shape model and its applications. *Computer Vision and Image Understanding*, 116(12):1178 – 1194.

Yazdanpanah, A., Hamarneh, G., Smith, B. R., and Sarunic, M. V. (2011). Segmentation of intra-retinal layers from optical coherence tomography images using an active contour approach. *IEEE Transactions on Medical Imaging*, 30:484–496.